Journal of Theoretical and Applied Vibration and Acoustics 10 (2) 50-76 (2024)

I S A V

Journal of Theoretical and Applied Vibration and Acoustics

journal homepage: http://tava.isav.ir

Exploiting an arc-shaped rotary magneto-piezoelastic energy harvester: Theoretical and experimental investigations

Iman Fakhari Golpayegani [a,b,*], **Ali Asghar Jafari** [a]

[a] *Faculty of Mechanical Engineering, K.N. Toosi University of Technology, Tehran, IRAN*

[b] *Mechanical Engineering Group, Golpayegan College of Engineering, Isfahan University of Technology, Golpayegan, IRAN*

Research Article

ARTICLE INFO

Article history:
Received 17 September 2024

Received in revised form 2 December 2024

Accepted 4 January 2025

Available online 17 February 2025

Keywords:

Rotational energy harvester

Arc-shaped

Piezoelectric

Nonlinear magnetic force

Frequency up-conversion

Sub-harmonic vibration

ABSTRACT

This article investigates a new piezoelectric harvester for extracting energy from rotational motions. The harvester's geometry is selected as a curve to increase the energy harvesting density. For its optimal performance across a wide range of rotational speeds, the harvester is excited by a non-linear magnetic force. Simultaneously with the rotation of the shaft and the attached magnet and creating a magnetic force, the magnet at the tip of the beam is excited, causing the curved piezoelectric element installed in the harvester to repeatedly deform and generate electrical energy. Electromechanically coupled differential equations are developed based on Hamilton's principle, and the Lagrange equations and piezoelectric relationships are extracted and numerically solved. This research accurately calculates the force between the magnetic dipole and a new time and displacement-dependent correction factor. This model is used to investigate how the output voltage and power of the harvester are affected by the rotational speed, magnetic gap, number of excitation magnets, and circuit resistance in both the time and frequency domains. Most significantly, the theoretical modeling results are compared with experimental data obtained from constructing a prototype and conducting numerous tests. The results indicate that reducing the magnetic gap and increasing the number of magnets to a certain extent will increase the voltage and output power. The maximum power and maximum power density extracted during excitation with four magnets at a rotational speed of 986 rpm are 1523.5 μW and 11.37 μW/mm^3, respectively, demonstrating the superior performance of the designed system.

* Corresponding Author:
E-mail Address: fakhari@email.kntu.ac.ir (I. F.Golpayegani)

https://dx.doi.org/10.22064/tava.2025.2041355.1248

1. Introduction

Energy harvesting from mechanical motions is one of the renewable, sustainable, and reliable sources for replacing or extending the life of batteries. Mechanical movements can be broadly categorized into vibration, fluid motion, and rotation. Combining these motions with advanced piezoelectric materials allows a suitable combination for high-density energy harvesting, simple structure, and long-term maintenance-free operation.

Piezoelectric energy harvesting systems coupled with rotational motions can be used for electrical energy harvesting, condition monitoring of rotating machinery, and sensors for measuring fluid flow and speed. Numerous studies have been conducted in this field. Ramazan Pour et al.[1] developed and evaluated a rotating piezoelectric harvester comprising eight fixed bimorph beams and one rotated beam to harvest energy from environments with low frequency and high amplitude. The effect of rotational speed and the orientation of the beams, both horizontally and vertically, on the extracted energy was investigated. Cho et al.[2] developed a hybrid electromagnetic-piezoelectric harvester for energy harvesting from a household water pipeline system. The average extracted magnetic power was 648 mW, and the piezoelectric power was 0.196 mW, used to operate a smart water meter and a water leak detection system through the Internet of Things, respectively. Makado et al.[3] designed, analyzed, and tested a rotating piezoelectric harvester in the 0.7 to 2.5 Hz frequency range. A Non-resonant excitation method was used to enhance performance, resulting in a power harvesting set with an 80% efficiency capable of extracting 845 μW. Egbe et al.[4] fabricated and tested the hybrid rotational energy harvester comprising piezoelectric, triboelectric, and electromagnetic generators for energy harvesting from low-wind speeds. The maximum electrical power was obtained as 121 μW, 191 μW, and 168 nW for the piezoelectric, EM, and triboelectric components at the wind speed of 3.5 m/s, respectively. Lo and Sho [5] studied a piezoelectric frequency up-converted energy harvester with a self-powered synchronized electric charge extraction interface circuit. The harvester device comprised a piezoelectric cantilever beam whose tip magnet was impulsively excited by another magnet fixed on a rotating plate. They developed a theoretical model based on the Fourier decomposition of magnetic force to realize the phenomenon of frequency up-conversion. A rotational impact generator, including two harvester beams with an auxetic structure and one exciting beam, was designed and tested for energy harvesting from low-frequency sources by Fang et al.[6]. Due to the centrifugal force and gap from the harvester beam, the impact force of the exciting beam created voltage in the piezoelectric materials, which, by adjusting this gap, made it possible to change the output power. The influential factor in improving the efficiency of the assembly was the rotational-centrifugal-softening effect, resulting in a maximum power and energy harvesting density of 0.673 mW and 41.23 W/g, respectively.

In recent years, extensive research has been conducted on various types of linear piezoelectric harvesters in terms of geometry, structure, excitation type, and materials [7-10]. These harvesters can extract considerable electricity during their resonance, but their power output is typically very low outside that range. However, mechanical motions and rotations of environmental sources are distributed across a wide range of frequencies [11]. Considering the high frequency of the harvesters [12] and the low frequency of environmental energy sources [13], it is necessary to optimize the harvester systems [14]. One proposed solution to this issue is the nonlinear optimization of the energy harvesting system by increasing the stability points of the system [15-17] and magnetic excitation. In this case, in addition to extracting high voltage at the system's

natural frequency, high voltage can also be harvested through sub-harmonic generation [18]. However, the amount harvested will be less than that at resonance. This phenomenon and energy harvesting systems are known as frequency up-conversion and non-resonance energy harvesting systems [14]. Sari et al.[19] designed an electromagnetic generator consisting of 20 series beams, effectively harvesting energy from 70 to 150 Hz from environmental vibrations. One of the beams could produce a voltage of 0.57 mV with a power of 0.25 nW in the frequency range of 95 to 2000 Hz. In the study by Fu and Yateman [20], a theoretical model with distributed parameters was presented for analyzing the electromechanical behavior of a rotational energy harvester. This system included a Unimorph beam with a tip magnet and a rotating magnet on a rotating disc, achieving energy harvesting using the frequency up-conversation method. Various excitation configurations were investigated to improve the device's output power. Wu et al.[21] conducted energy harvesting from rotational mechanisms with a combination of magnetic attraction and repulsion. Non-contact excitation was used to reduce friction and energy loss, resulting in a power of 1.23 mW at a rotating frequency close to the natural frequency of the harvester. Finite element analysis using ANSYS software and experimental testing of a piezoelectric wind turbine with dimensions of $25 \times 35 \times 80mm^3$ were performed by Silwa et al.[22]. The device consists of three magnets arranged at 120-degree angles on an axis connected to a propeller rotated by the wind, and each magnet individually excited a separate beam. Numerous analyses were conducted to reach the optimal dimensions of the generator, obtaining powers of 2.06 mW for a single beam and 3.78 mW for three beams in parallel. In the most recent work, by Rizal et al.[23], a harvester consisting of an octagonal rotating disk was presented. Each edge of the disk had a flexible plate, a piezoelectric layer, and a magnet, and four stationary beams with tip magnets stimulated these layers. This research simplified the electrical power, voltage, and periodic magnetic force relationships between the magnets. The magnetic force has been equivalenced to a Fourier series. The maximum instantaneous voltage in series mode ranged from 14 to 19 volts, and in parallel mode, it ranged from 7.5 to 8 volts, and the power density extracted was over 9.67 μW/mm3. Kao et al.[24] used a bistable rotating beam for harvesting electrical energy. An experimental sample was constructed and compared with the numerical results. The optimum efficiency of this system was achieved at rotational speeds between 300-550 rpm, producing an average voltage of 9.44 volts at 540 rpm.

Improving the energy harvesting density by modifying the geometry of energy harvesters is achievable. Geometric modifications lead to a more uniform distribution of strain and electric charge, less concentration of stress at the support, and, consequently, an increase in the system's life. Extensive research has been conducted on geometry enhancement, mainly modifying rectangular beam geometries [24-29]. However, the use of curved-shaped harvesters significantly increases energy harvesting density due to having a larger high-strain region than flat ones [30-34]. Jang et al.[35] used an arc-shaped device to convert human motion into electrical energy. This assembly produced a maximum voltage of 120 V with a current intensity of 700 μA in one cycle and demonstrated power harvesting capabilities at very low frequencies up to 1 Hz. A cantilever curved beam, consisting of a substrate layer and a piezoelectric layer, was investigated by Yang et al.[30] using the finite element method and experimental studies. Castigliano's second theorem was employed to determine the load-displacement curve, and Euler-Bernoulli assumptions were considered in the software. The results showed that the maximum stress region in the curved beam was higher than in the straight beam. Due to a relatively more uniform stress distribution and less redistributed charge effects in the proposed model, higher voltage, power, power density, and

efficiency were achieved. Experimental data indicated that arc-shaped PEHs could produce 2.55-4.25 times more than flat PEHs. Furthermore, Zhao et al.[36] extended this work using linear Timoshenko theory with the mode expansion method. To increase energy harvesting, they added a concentrated mass to the end of the beam. They investigated the effects of the length of the straight section of the beam and the thickness ratio on the energy harvesting amount. Chen et al. presented a nonlinear bistable curved-straight harvester composed of a curved-straight beam.[32] and experimentally validated. The bandwidth of this system was higher compared to linear harvesters, and in optimal resistance, compared to a straight beam, it produced 40% and 72% higher voltage and power density, respectively. Ding et al.[37] designed an array of harvesters consisting of five curved-straight beams. Due to a slight difference in the radius of curvature in the curved section of the harvester, the beams had different but close natural frequencies, resulting in an increased bandwidth of energy harvesting from 7 Hz in a single-beam harvester to 53 Hz in the array configuration. Analysis, finite element modeling, experimentation, and comparison of curved and straight harvesters were performed in the study by Krishnan et al.[33]. The most crucial parameter investigated in this research was the effect of the central angle of the curve on the maximum voltage, and an optimal range of 130-160 degrees was obtained. Chen et al.[38] designed a composite harvester consisting of two arc-shaped structures, a flat section, and two concentrated masses. They validated the theoretical model with finite element results and extracted the effects of geometric parameters, excitation range, and resistance load on the harvested energy. The combination of softening and hardening nonlinear behavior increased the bandwidth of the proposed design. Experiments demonstrated an increase of 225% and 450% in voltage and output bandwidth, respectively, compared to a flat double-clamped beam. Shang et al. [39] proposed a novel energy harvester that consists of a piezoelectric inverted beam and two arc-shaped branches. The harvester has the characteristics of super-harmonic and subharmonic vibrations, which significantly extends its working frequency bandwidth. The results demonstrated that the harvester can produce a substantial electric output under weak stochastic excitations.

From the mentioned sources, it can be inferred that curved-shaped energy harvesters produce higher power and voltage density than their straight counterparts. Additionally, energy harvesting is feasible at low frequencies due to the nonlinearity introduced by the magnetic excitation and frequency up-conversion. The combination of curved beams and nonlinear magnetic force is expected to yield significant results in increasing the amplitude and bandwidth of energy harvesting. Notably, research on energy harvesting from rotating systems employing curved beams has yet to be conducted. Therefore, in this study, a nonlinearly magnetically excited curved piezoelectric harvester has been designed, analyzed, and experimentally studied. The magnetic force is precisely calculated, and the coupled electromechanical equations are derived and solved to determine the effects of the number of magnets, circuit resistance, magnet distance, and rotation speed on the system response. Theoretical and experimental results are in perfect agreement due to time and displacement-dependent magnetic correction factors. This system can function over a wide range of rotational speeds with a broad bandwidth, and it can be compatible with most energy harvesting methods, such as fluid motion and rotating machinery.

2. The proposed energy harvester

With the aim of high-density energy harvesting at different excitation frequencies, a piezoelectric harvester that utilizes the vibration of a curved piezoelectric beam to harvest energy from rotational movements has been developed. The illustrated harvesting assembly in Figure 1(a) consists of a heavy metal base, an electric motor, bearings, an energy harvester, and guide rods. As shown in Figure 1(b), the Arc shaped Rotational Piezoelectric Energy Harvester (ARPEH) also includes a curved piezoelectric Unimorph beam, a tip magnet, an exciting magnet, and an octagonal rotating disc capable of housing eight magnets. A flexible piezoelectric material made of polyvinylidene fluoride (PVDF) with a high piezoelectric coefficient is utilized as the energy-harvesting component. This material can withstand significant deformations across a wide range of frequencies, which helps to improve energy conversion efficiency. Figure 2 illustrates the geometric parameters used in ARPEH for the driving theoretical formulation, finite element modeling, and prototype manufacturing. The thicknesses of the substrate and piezoelectric layer, the beam width, the internal radius of the curved beam, and the total length of the harvester are denoted by h_S, h_P, b_0, r_i, and L, respectively. The magnets' length, width, and height are represented by a, b, and h, respectively. The radius of the placement of magnets on the eight-sided disc is R_D, and the distance between two magnets (magnet gap) at $\alpha = \pi/2$ and in the undeformed state of the beam is d_m.

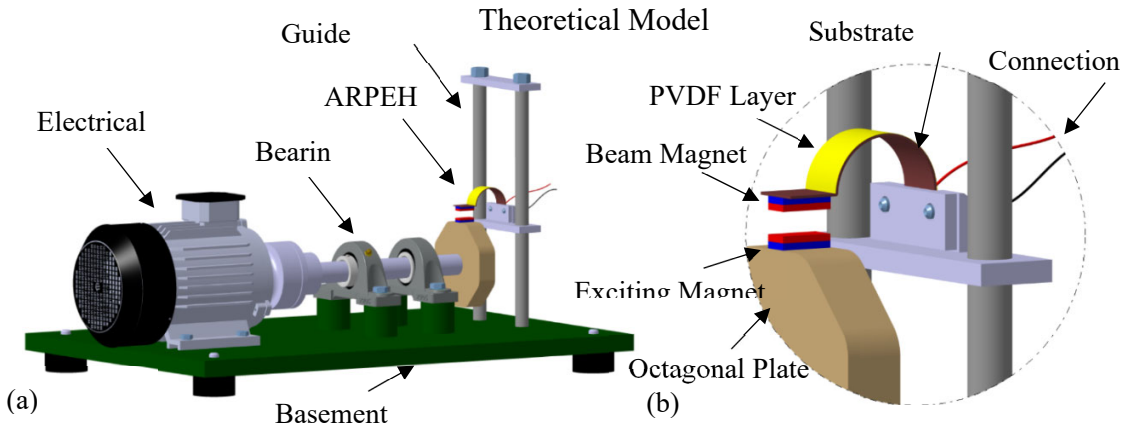

Fig. 1: (a) Energy harvesting system and (b) Arc-shaped rotary-based piezoelectric energy harvester (ARPEH)

The performance of the proposed system is as follows: Due to the rotation of the axis, the magnet attached to the disk rotates, and due to the opposing poles being placed against each other, a repulsive force is created between the magnets, which is followed by a periodic nonlinear magnetic force applied to the end of the beam. The beam oscillates until the excited magnet re-excites, resulting in the generation of electrical energy output. The developed energy harvester can produce sufficient energy and does not require matching the excitation frequency to the resonance frequency. Furthermore, by adjusting the number and dimensions of the magnets, rotation speed, dimensions of the octagonal disk, and position of the piezoelectric beam, a wide range of beam oscillations can be achieved, allowing the energy harvester to generate electricity effectively.

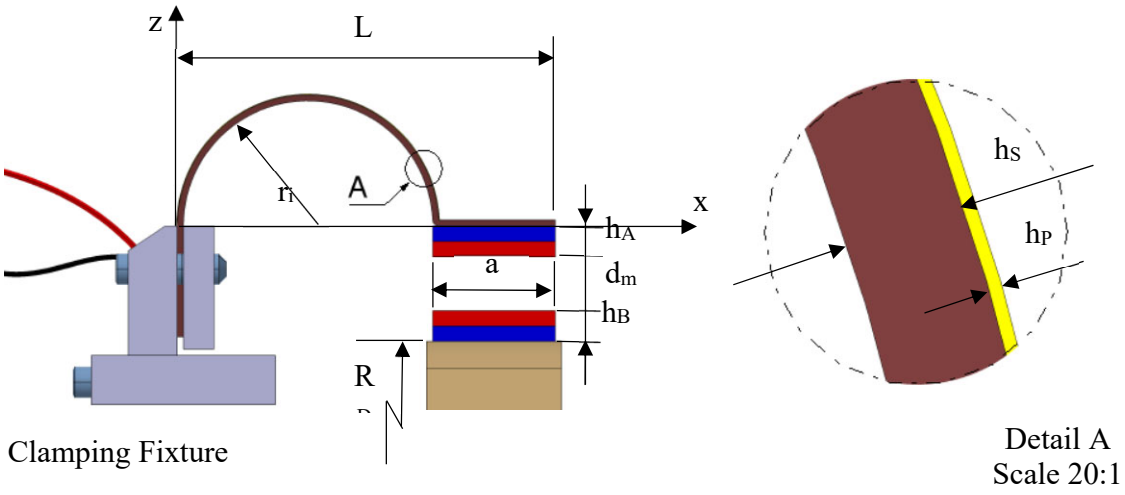

Fig. 2: ARPEH dimensions

3. Theoretical modeling of the ARPEH

3.1. Energy equation

The Lagrange equations, developed to derive the coupled electromagnetic equations of the ARPEH system based on the Hamiltonian principle, are utilized [40]:

$$\int_{t1}^{t2}(\delta T - \delta U + \delta W_{ie} + \delta W_{nc})dt = 0, \tag{1}$$

where T is the total kinetic energy, U is the total potential energy, W_{ie} is the internal electrical energy, and W_{nc} is the virtual work of generalized non-conservative forces, including mechanical, damping, and electric charge components. The kinetic energy of the harvester includes the sum of the kinetic energy of the curved beam T_S, the piezoelectric layer T_P, and the end magnet T_M, determined by the following equations :

$$T = T_S + T_P + T_M \tag{2}$$

$$T_S = \frac{1}{2}\int_{V_S}\rho_S \dot{w}^2(x,t)dV_S \tag{3}$$

$$T_P = \frac{1}{2}\int_{V_P}\rho_P \dot{w}^2(x,t)dV_P \tag{4}$$

$$T_M = \frac{1}{2}M_t \dot{w}^2(x,t)|_{x=L} + \frac{1}{2}I_t\left[\frac{\partial^2 w(x,t)}{\partial t \partial x}\Big|_{x=L}\right]^2 \tag{5}$$

In the above equations, $w(x.t)$ is the transverse displacement of the beam, ρ_S and ρ_P are the density of the metal substrate, and the piezoelectric layer, V_S and V_P are the volumes of the metal substrate and the piezoelectric layer, M_t is the magnet mass, and I_t is the moment of inertia of the magnet about its free end. Considering the harvester oscillation in the z-direction, the piezoelectric constitutive equations are given by [41]:

$$T_1 = \bar{C}_{11}^E S_1 - \bar{e}_{31}E_3 \tag{6}$$

$$D_3 = \bar{e}_{31}S_1 + \bar{\varepsilon}_{33}^S E_3 \tag{7}$$

where T_1 and S_1 are the stress and strain in the beam length direction, $\bar{C}_{11}^{E}$ is the Young's modulus, $\bar{e}_{31}$ is the coupling coefficient, and $\bar{\varepsilon}_{33}^{S}$ is the dielectric permeability at the constant strain of the PVDF layer. Also, D_3 and E_3 represent the electric displacement and the electric field, respectively. After rewriting the electric field based on the piezoelectric voltage, which is equal to $E_3 = -v(t)/h_P$, the electric energy generated by PVDF is given by:

$$W_{ie} = \frac{1}{2}\int_{V_P} E_3 D_3 dV_P = \frac{1}{2}\int_{V_P} \frac{-v(t)}{h_p}(\bar{e}_{31}S_1 - \bar{\varepsilon}_{33}^{S}\frac{v(t)}{h_p})dV_P = -\frac{1}{2}\frac{v(t)}{h_p}\bar{e}_{31}\int_{V_P} S_1 dV_P + \frac{1}{2}C_P v^2(t) \quad (8)$$

In the above equation, $C_P = \bar{\varepsilon}_{33}^{S} bL_P/h_P$ is called the capacitance of the PVDF layer. For simplicity, the damping coefficient C_d is considered constant for the system [36]. The virtual work of non-conservative forces and electric charge due to electrical resistance can be calculated by:

$$W_{nc} = \int_{V_S} -c_d w(x,t)\dot{w}(x,t)dV_S + Q(t)v(t) \quad (9)$$

where $Q(t)$ and $v(t)$ are PVDF's electric charge and voltage, respectively. By substituting the above equations into Equation (1), the Lagrange equation is derived as follows:

$$\frac{d}{dt}\left(\frac{\partial T}{\partial \dot{q}_k}\right) - \frac{\partial T}{\partial q_k} + \frac{\partial U}{\partial q_k} - \frac{\partial W_{ie}}{\partial q_k} - \frac{\partial W_{nc}}{\partial q_k} = 0 \qquad k = 1,2 \quad (10)$$

In this equation, q_k represents the generalized modal coordinates and voltage. The potential energy of the harvester is the sum of the magnetic potential energy due to the magnets U_M and the strain potential energy of the harvester U_{ARPEH} given by:

$$U = U_M + U_{ARPEH} \quad (11)$$

According to Equation (10), the result of taking the derivative of the total potential energy of the system will be the magnetic force F_M and the ARPEH restoring force F_r.

$$F_r = \frac{\partial U_{ARPEH}}{\partial q_k} \quad (12)$$

Therefore, in sections 3.2 and 3.3, the values of these two forces will be determined based on the harvester's mechanical, magnetic, and geometric specifications.

3.2 Modeling of magnetic force

Many studies have used a simplified form of the magnetic force. For example, as a triangular pulse without considering the slope at the beam's end [20, 23, 42, 43]. Therefore, in this article, the detailed version of nonlinear magnetic force is considered to increase the accuracy of the results. This will lead to a very close approximation to the physics of the problem and consequently yield better alignment with test results and modeling. The magnetic potential energy and force applied by magnetic dipole A on magnetic dipole B can be obtained as follows [44]:

$$U_M = -\frac{\mu_0}{4\pi}\left(\vec{\nabla}\frac{\vec{m}_A\cdot\vec{r}_{AB}}{\|\vec{r}_{AB}\|_2^3}\right)\cdot\vec{m}_B \quad (13)$$

$$\vec{F}_{BA} = -\frac{\mu_0}{4\pi}\vec{\nabla}\left[\left(\vec{\nabla}\frac{\vec{m}_A\cdot\vec{r}_{AB}}{\|\vec{r}_{AB}\|_2^3}\right)\cdot\vec{m}_B\right] = -\frac{\mu_0}{4\pi}\vec{\nabla}\left[\frac{\vec{m}_A\cdot\vec{m}_B}{\|\vec{r}_{AB}\|_2^3} - 3\frac{(\vec{m}_A\cdot\vec{r}_{AB})(\vec{m}_B\cdot\vec{r}_{AB})}{\|\vec{r}_{AB}\|_2^5}\right] \quad (14)$$

where μ_0 is the permeability of free space, $\overrightarrow{r_{AB}}$ is the vector connecting the centers of magnetic dipoles A and B. Also, $\overrightarrow{m_A}$ and $\overrightarrow{m_B}$ are the magnetic moment vectors of magnetic dipoles A and

B, respectively, obtained from the product of the volume of permanent magnet v and the magnetizing vector $\vec{M}$.

$$\vec{m} = \vec{M} \cdot V \tag{15}$$

In this relation, the size of the magnetizing vector can be approximated using B_r, which is the magnetic flux density, as $M \cong B_r \mu_0 (A/m)$ [2]. The details of the force applied from the exciting magnet to the excited magnet are shown in Figure 3. According to Figures 3b and 3c, the magnetic vectors of the exciting (B) and excited (A) magnets are derived from Equation (16), respectively:

$$\vec{m}_B = (M_B V_B \, cos(\alpha))\hat{j} - (M_B V_B \, sin(\alpha))\hat{k}$$
$$\vec{m}_A = (M_A V_A \, sin(\gamma))\hat{i} - (M_A V_A \, cos(\gamma))\hat{k} \tag{16}$$

In this equation, α is the angle of the magnetic moment vector of the exciting magnet with the stationary Y-axis. The angle of the magnetic moment vector of the excited magnet concerning the Z-axis is denoted by γ. In the presence of a magnet on the disc, the angle α is given as follows:

$$\alpha = \alpha_0 + \frac{n\pi}{30} t \tag{17}$$

where α_0 is the angle of the magnet at the moment of starting the motion, the vector $(\overrightarrow{r_{AB}})$ determines the distance from the magnetic moment source to the excited magnet at each instant. It should be noted that α depends on the rotational speed of the axis n (rpm) and the period of force application $\bar{T} = 60/n \; (s)$.

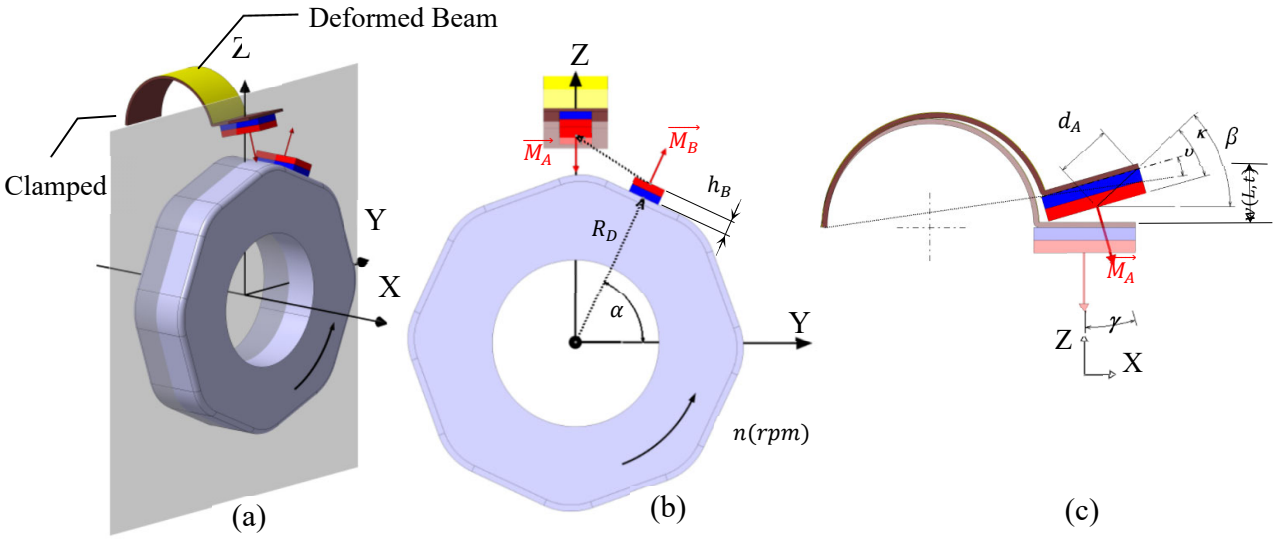

Fig. 3: Parameters used for modeling nonlinear interaction due to permanent magnets. (a) Isometric view, (b) Front view, and (c) Geometric distances and angles

$$\vec{r}_{AB} = (\frac{a}{2} - d_A \, cos(\beta))\hat{i} - R_B \, cos(\alpha)\hat{j} + (R_A + w(L,t) - d_A \, sin(\beta) - R_B \, sin(\alpha))\hat{k} \tag{18}$$

The magnetic force vector will be derived by substituting Equations 15 to 18 into Equation 14. The transverse force component for the beam is obtained as follows:

$$\bar{F}^Z{}_{AB} = \frac{3\mu_0 M_A V_A M_B V_B}{4\pi A_5^2}$$

$$\begin{Bmatrix}[\big(2-5(A_1^2+A_3^2)\big)(A_2-A_4)\,cos(\beta-\kappa)+(1-5(A_2-A_4)^2)A_1\,sin(\beta-\kappa)]\,sin(\alpha)+\\ [(1-5(A_2-A_4)^2)A_3\,cos(\beta-\kappa)+5(A_2-A_4)A_1A_3\,sin(\beta-\kappa)]\,cos(\alpha)\end{Bmatrix} \quad (19)$$

In Equations (18) and (19), $w(L.t)$ is the displacement of the beam end in the Z-axis, R_B is the distance from the rotation axis to the magnetic vector application point of the exciting magnet, d_A is the distance from the magnetic vector application point to the opposite end of the excited magnet, v is the slope of the beam end, κ is the angle formed by d_A, and β is the angle of d_A with the X-axis. The calculation method for these values, along with the constants $A_i.\, i = 1.\ldots.5$, is provided in Appendix A. Equation (19) is valid for the case where only one magnet is on the disc and in the energy harvesting mode with excitation by n_0 magnets, the Heaviside function is used to express the magnetic force:

$$F_{AB}^{Z} = \sum_{i=0}^{J}\Big[\big(Heaviside(t-i\cdot T)-Heaviside(t-i\cdot T-2T_m)\big)\cdot \begin{cases}\bar{F}_{AB}^{Z} & i\cdot T<t<i\cdot T+2T_m\\ 0 & otherwise\end{cases}\Big] \quad (20)$$

where J is the number of loading cycles, $T = 60/n_0 n$ (s) is the force application period, $T_m = 60\theta/n_0 n$ (s) is the excitation time [42], and θ (rad) is the central angle of the arc when two magnets are in each other's effective magnetic field. According to Figure (4), the exciting magnet reaches position B from position A.

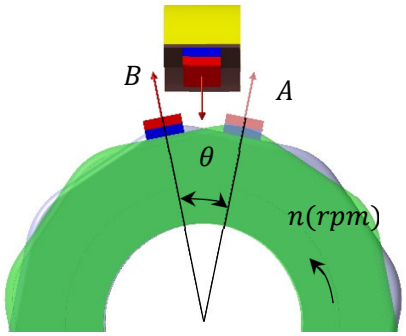

Fig. 4: Excitation progress

A crucial point in the force relationships is that Equation 14 has high accuracy when the ratio of the distance between the magnets to the magnetic moment radius of each magnet is greater than 10 [44]. Since this ratio is small in magnetic energy harvesting systems, a correction factor needs to be considered for Equation 20. Because the magnetic moment of each magnet has a constant radius while the distance between the magnets varies during energy harvesting, the ratio mentioned is also variable. As a result, the correction factor mentioned will depend on the varying distance. In energy harvesting studies with magnetic force, this factor has either yet to be considered [1, 45-47] or has been taken as a constant [23, 32, 43]. Thus, the maximum force between two magnets was determined experimentally based on their distance and then compared with the maximum extracted force in the theoretical method, and the following relationship is used as the correction factor.

$$\bar{K} = -8796\bar{z}^2 + 898.19\bar{z} - 2.3649 \quad (21)$$

In Equation 21, the minimum distance between the magnets during the oscillation of the curved beam is given by $\bar{z} = \sqrt{A_1^2 + (A_2 - R_D - h_B)^2}$, where h_B represents the height of the exciting magnet. The corresponding plots for this correction factor are presented in section 6.2. Finally, the magnetic force applied to the end of the energy harvesting beam will equal the product of the extracted force in Equation (20) and the correction factor in Equation (21).

3.3. Modeling the nonlinear restoring force of ARPEH

Due to the harvester's geometric curvature and composite structure comprising a copper beam and piezoelectric polymer, the relationship between the restoring force and displacement along the z-axis at the beam's end is nonlinear. Specifically, relative to the static equilibrium position, the force magnitude is less when the beam moves in a positive z-direction than when it moves in a negative z-direction. The reason for this lies in the neutral axis not coinciding with the geometric axis of the beam and its curvature change during deformation. An experimental approach was implemented to capture the force-displacement curve at the beam's end. In this setup, one beam end is securely fixed in a fixture, while the other is linked to a dynamometer for measuring the restoring force at various displacements [32, 48]. As illustrated in Figure 5, the experiment is repeated multiple times to improve the accuracy of the results, and the average results are used to calculate the restoring force.

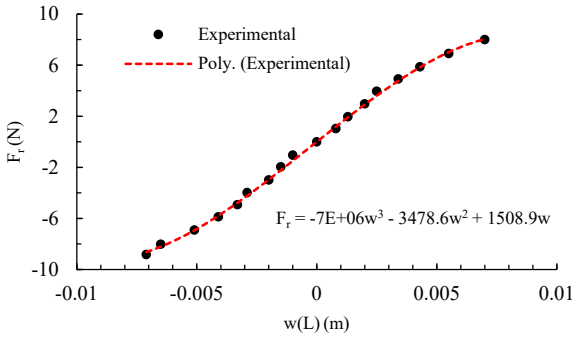

Fig. 5: The nonlinear restoring force curve of the harvester

According to the obtained results, it is evident that a third-degree polynomial precisely aligns with the data points. The equation can be expressed as follows:

$$F_r = k_3 w^3(L,t) + k_2 w^2(L,t) + k_1 w(L,t) \tag{22}$$

where $k_1 = 1508.9N/m$, $k_2 = -3478.6N/m^2$, and $k_3 = -7e6N/m^3$ indicate that the harvester has exhibited softening behavior.

3.4. Coupled electromechanical equations

This section introduces a formal solution method for the coupled electromechanical equations governing an arc-shaped energy harvester. In-plane vibration and perpendicular to the harvester can be represented through a series of absolute and uniformly convergent eigenfunctions.

$$w(x,t) = \sum_{r=1}^{\infty} \varphi_r(x)\eta_r(t) \tag{23}$$

Here, $\varphi_r(x)$ and $\eta_r(t)$ represent the mass normalized mode shape function and modal coordinates of r^{th} mode, respectively. Because of the low frequency in the exciting magnet's rotational motion, which closely approaches the first natural frequency of the beam, the predominant mode is the first. Consequently, modeling is conducted by considering only the first mode for the relevant boundary condition, denoted as $\varphi_1(x) = 1 - \cos(\pi x/2L)$. This function is a typical approximate function used for clamped-free boundary conditions [32, 47].

Considering the generalized coordinates $\eta(t)$ and $v(t)$ and substituting the relationships from Equations 2, 8, 9, 20, 21, 22, and 23 into Equation 10, the coupled electromechanical equations of the ARPEH are derived.

$$M\ddot{\eta}(t) + C_d\dot{\eta}(t) + k_3\eta^3(t) + k_2\eta^2(t) + k_1\eta(t) - \chi v(t) = \bar{K}F_{AB}^{Z}\delta(x-L) \tag{24}$$

$$C_P\dot{v}(t) + \frac{v(t)}{R_L} + \chi\dot{\eta}(t) = 0 \tag{25}$$

In this correlation, δ is the Dirac delta function, and M and C are the approximate modal mass and damping of the ARPEH, respectively, expressed as:

$$M = \rho_S b_0 h_S \int_0^{L_S} \varphi^2(x)\,dx + \rho_P b_0 h_P \int_0^{L_P} \varphi^2(x)\,dx + \frac{1}{2}M_t\varphi^2(L) - I_t\varphi'^2(L) \tag{26}$$

$$C = \int_0^L c_d\varphi^2(x)dx \tag{27}$$

where $\zeta = \int_0^L (C_d/2M\omega)\varphi^2(x)dx$ and ω is the fundamental natural frequency. Furthermore, χ represents the electromechanical coupling term, and R_L denotes the circuit resistance.

$$\chi = b_0 e_{31} h_{pc} \int_0^{L_P} \left(\frac{d^2}{dx^2}\varphi(x)\right) dx \tag{28}$$

Here, the defining relationship for the distance from the neutral axis to the centerline of the piezoelectric layer, denoted as h_{pc}, is expressed in Appendix A. Section 6 provides an in-depth overview of the results obtained by solving Equations (24) and (25), which determine the displacement and output voltage of the piezoelectric material.

4. Finite element modeling of the ARPEH

A comprehensive finite element model of the ARPEH was simulated using ANSYS APDL software. The substrate layer was modeled using Solid 186 elements with Cartesian coordinate systems. The piezoelectric layer employed was modeled using Solid 226 elements with cylindrical

coordinate systems $(r.\theta.z)$ aligned with the polarization direction (r). One end of the beam is fully constrained, and on the other side, the magnetic force is applied based on Equations (20) and (21). The results of the harmonic analysis performed to extract linear natural frequencies are provided in section 6.1, compared with the results of the modeling and experimental setup.

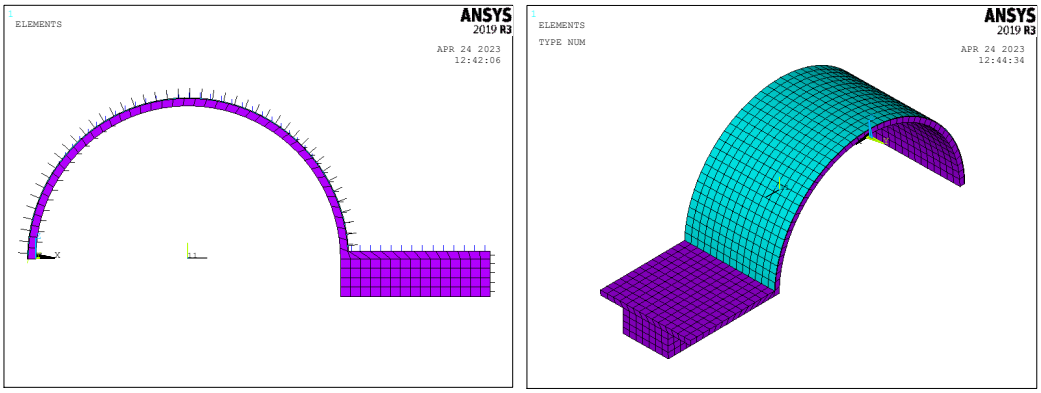

Fig. 6: Geometry of FEM model of ARPEH

5. Experimental setup

As illustrated in Figure 7(a), an energy harvesting setup was constructed and experimentally validated to corroborate the analytical and finite element results. This setup consists of two main components: rotational actuation and energy harvesting. To establish the rotational system, an AC electric motor (ABB) is initially installed on a heavy-duty anti-vibration mount, accompanied by two bearings and two guide rods for stability, as depicted in Figure 7(d). A frequency inverter (LS) is connected to control the rotational speed. Before installing the energy harvesting equipment, the rotational shaft run-out was investigated to ensure the uniformity of the magnetic force applied to the end of the harvester. As depicted in Figure 7(e), this value was equal to 0.01 mm, ensuring accurate results extraction.

The second assembly, or the energy harvester itself, has been constructed with the specifications outlined in Table (1). An eight-sided disk and exciting magnets (ND 42) are mounted on a shaft to achieve this. A curved copper beam, affixed to a PVDF layer using Tesa adhesive (PolyK Technologies-PKS-P0110-Pin-001), shown in Figure 7(g), is fixed within guide rod fixtures. A resistance box (Figure 7(c)) is employed to investigate the impact of circuit resistance on voltage, and the output voltage is measured using an oscilloscope (MEGATEK-DSO5100) (Fig. 7(b)). The design of this setup is based on the magnetic repulsive force, and thus, the excited magnet (ND 42) is positioned at the end of the curved beam so that its N pole faces the N pole(s) of the magnet(s) attached to the disk.

Fig. 7: Experimental setup, (a) Complete setup; (b) Oscilloscope; (c) Resistance box; (d) Speed controller; (e) Run-out check (f) ARPEH; (g) PVDF layer

Table 1 Energy harvester parameters used in the simulations

Beam Feature	**Symbol**	**Value**
Length of substructure / PVDF	L_s/L_p	87 / 67 mm
Thickness of substructure /PVDF	h_s/h_p	1 / 0.11 mm
Widen of substructure / PVDF	b_0	20 mm
Inner radius of the beam	r_i	20.327 mm
Young modulus of substructure (Experiment) / PVDF[49]	E_s/E_p	102 / 2.5 Gpa
Density of substructure / PVDF [49]	ρ_s/ρ_p	8047 / 1780 Kg/m3
Piezoelectric constant [49]	d_{31}	-25 pmV^{-1}
Capacitance [49]	C_p	1.25 nF
Damping ratio (Experiment)	ζ	0.0204
Exciting/Excited Magnets Feature		
Dimensions	$a \times d \times h$	20×10×5 mm^3
Residual flux density	B_r	1.315 T
mass	M_t	7.415 gr
Rotating Cylindrical Plate Feature		
Diameter	R_D	38.75 mm
Max number of Magnets	$-$	8
permeability of free space	μ_0	$4\pi\times10^{-7}$

To ensure the optimal best match among simulation, finite element analysis, and experimental results, the elastic modulus and density of the copper substrate, along with the damping ratio, have been determined through experimentation. Given that the impulsive magnetic force is periodic, the damping ratio equals the free vibration damping ratio. To this end, the harvester is positioned on a fixture and mounted on a shaker (B&K Type 4809). The B&K data analysis software provides the corresponding data from measuring displacement, velocity, and acceleration using an Ometron VH300+ laser. The arrangement for conducting the damping and natural frequency tests is illustrated in Figure (8).

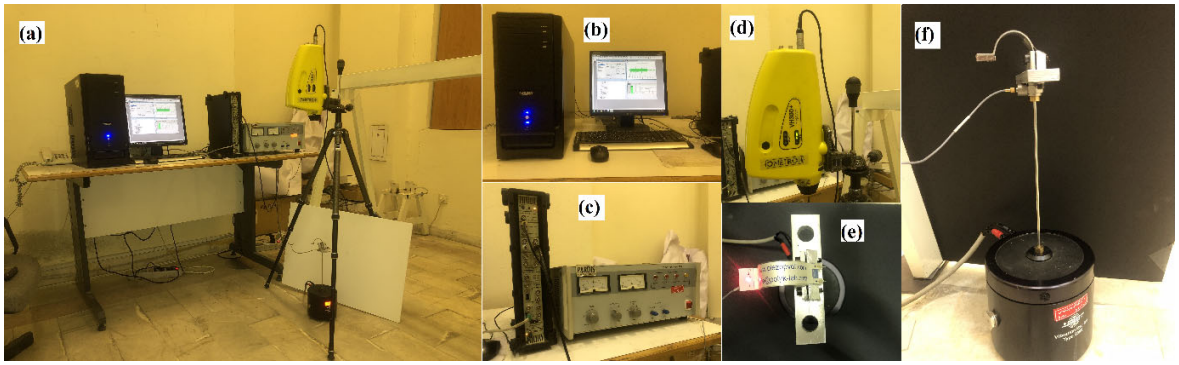

Fig. 8: Natural frequency and damping ratio experimental setup
(a) Complete setup; (b) B&K data analysis software; (c) Data acquisition system and amplifier; (d) Laser; (e) harvester; (f) Shaker

The shaker excites the harvester and is removed following a few seconds of excitation. After that, the damping ratio is calculated by plotting the displacement-time diagram. The average damping ratio is 0.0204 after ten iterations of this experimental procedure.

6. Results and discussion

6.1. Modal analysis validation

The compliance of the transverse mode shape and the system's natural frequency ($\omega = \sqrt{k_1/M}$) in analytical solutions and finite element analysis with the experimental results can be regarded as a criterion to ensure the reliability of the obtained data. To achieve this, Table (2) compares the results of the experimentally extracted Frequency Response Function (FRF) diagram with two other methods. Additionally, the transverse mode shape discussed in Section 3.4 is compared with the transverse component of the finite element model in Figure (9). Notably, the difference between the natural frequencies obtained from the finite element and analytical approaches and those from the experimental tests is slight. Concerning the transverse mode shape, as shown in Figure 5, the finite element results and the analytical method align well at the boundaries. However, they differ somewhat at the intermediate points due to the approximate nature of the mode shape. Therefore, it is reasonable to conclude that both theoretical modeling and finite element analysis are reliable for determining the vibration response of the system.

Table 2 Natural frequency comparison between theory, FEM, and experiment.

Fundamental Natural Frequency (ω)	Value (Hz)	Error (%)
Analytical	65.252	0.80
FEM	65.535	0.37
Experiment	65.780	– – – –

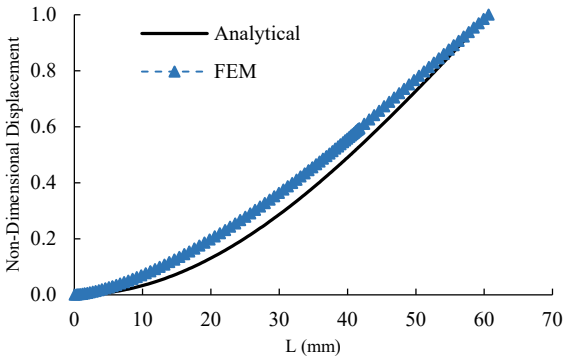

Fig. 9: Transverse mode shape comparison between theory and FEM

6.2. The magnetic force correction factor

Figure (10) illustrates the time and displacement-dependent magnetic force correction factor at the end of the harvester in the open circuit condition, based on Equation (21). A rotational speed of $n = \frac{\omega}{16} Hz = 245\ rpm$, and a distance between the magnets $d_m = 10\ mm$ have been considered. The plots illustrate that the correction factor varies based on the distance between the magnets. It reaches its maximum when the minimum distance between the exciting and excited magnets is considered. Consequently, adopting an average value for this correction factor may lead to errors in the results.

With an increase in the number of exciting magnets, the displacement at the end of the harvester rises, reducing the minimum distance between the magnets. As a result, both the maximum and average correction factor increase. For the case of eight exciting magnets, the maximum and average correction factors reach 6.165 and 9.15, respectively, compared to 5.839 and 7.25 for the case of one exciting magnet. Incorporating this variable correction factor represents an advantage of the present research compared to previous studies.

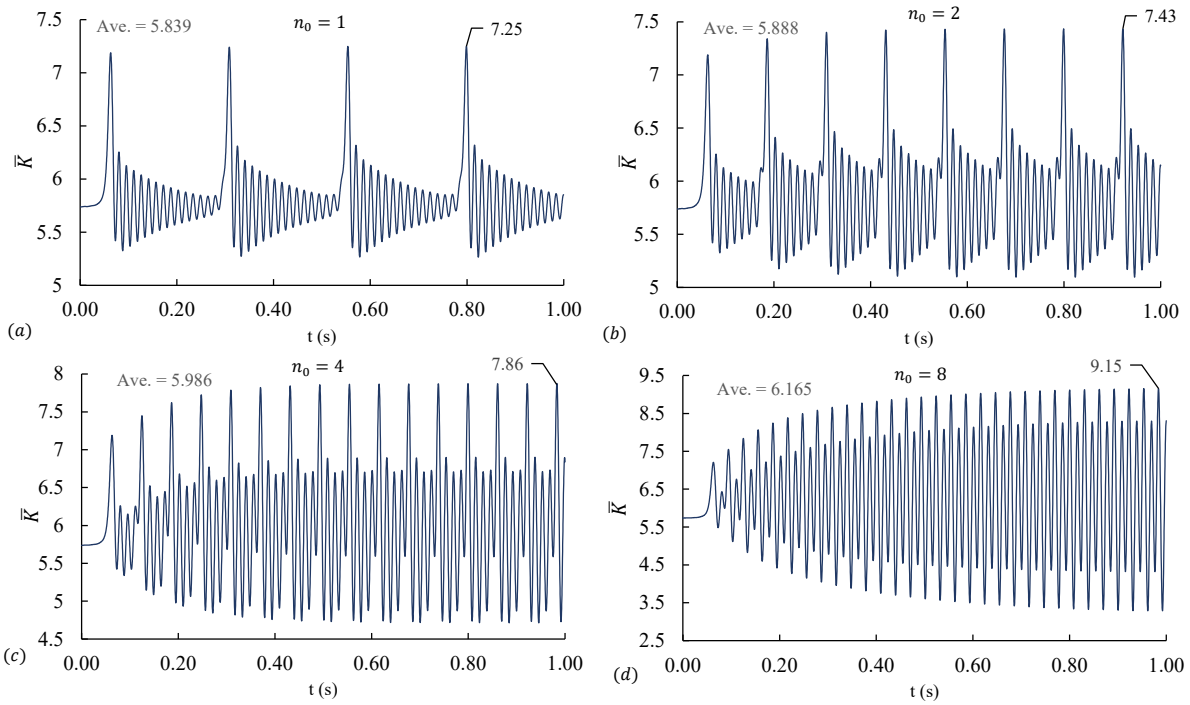

Fig. 10: Magnetic force correction factor, d_m=10 mm; n=ω/16 Hz=245 rpm
(a) n_0=1; (b) n_0=2; (c) n_0=4; (d) n_0=8

6.3. Time domain results

The initial comparison evaluates the theoretical model's capability to predict the harvester's performance over time. Figure (11) illustrates the open circuit voltage of the ARPEH with a magnet distance of $d_m = 10\,mm$ for two angular velocities and two magnet arrangements. As the rotational speed increases from 1/12 (326.3 rpm) in Figure 11(b) to 1/10 (391.5 rpm) in Figure 11(a) of the harvester's natural frequency in the configuration with one exciting magnet, the maximum voltage rises from 23.03 V to 31.11 V. Meanwhile, for the configuration with two exciting magnets, the maximum voltage changes from 38.26 V in Figure 11(d) to 43.97 V in Figure 11(c). As is well known, there is a strong alignment between the theoretical and experimental results in all four cases. The differences in maximum voltage for these cases are 0.3%, 2.1%, 7.33%, and 9.35%, respectively.

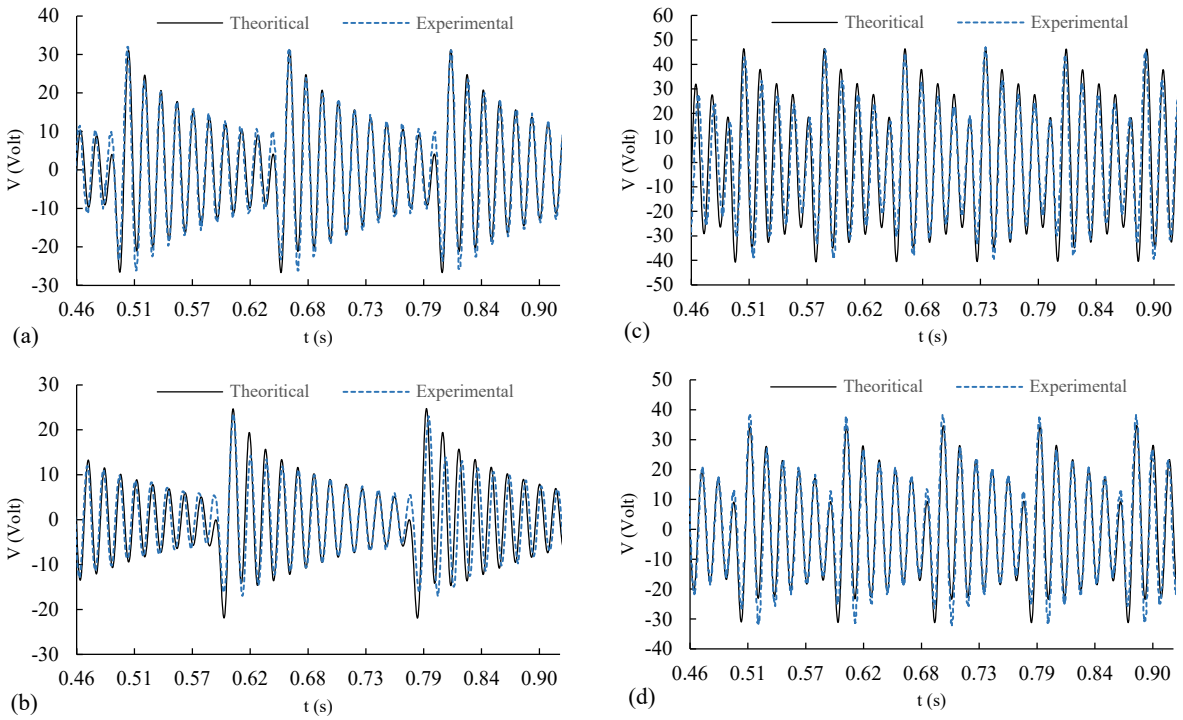

Fig. 11: Open circuit output voltage, d_m=10 mm
(a) n_0=1, n=ω/10(Hz); (b) n_0=1, n=ω/12(Hz); (c) n_0=2, n=ω/10(Hz); (d) n_0=2, n=ω/12(Hz)

6.4. Effect of rotational speed on ARPEH

This section compares the Maximum, RMS, and Peak-to-Peak voltages between the theoretical model and experimental results, as shown in Figure (12). The system is in open-circuit mode with a magnet distance of dm=10 mm. The effect of stepwise change of rotational speed from 217 to 450 rpm (multiples of the natural frequency of the harvester, i.e., $\frac{\omega}{i}$; i = 8.9.10.11.12.14.16), and the variation in the number of exciting magnets from one to two are illustrated on the output voltages. The increase in rotational speed enhances the Maximum, Average, and Peak-to-Peak voltages, with the percentage increase being more noticeable in the RMS voltage.

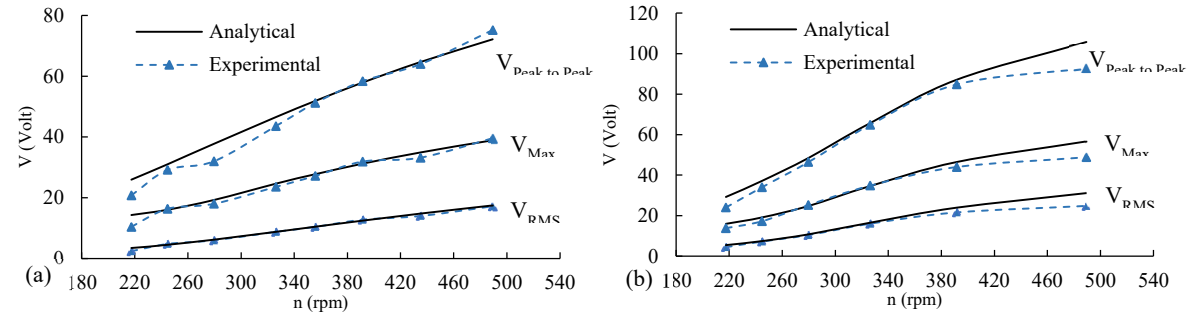

Fig. 12: Open circuit output voltage, d_m=10 mm, (a) n_0=1; (b) n_0=2

In the configuration with one exciting magnet shown in Figure 12(a), the Maximum, Average, and Peak-to-Peak voltages vary in the ranges of ۱.39–38.93 V, 3.45–17.47 V, and 25.94–72.17 V, respectively, with a significant 406% increase in the average voltage. As shown in Figure 12(b), in the case of excitation with two magnets with a 180-degree angle between them, these values range from 13.47–56.64 V, 4.18–31.14 V, and 23.42–105.70 V, respectively, with a 644% increase in the average voltage. A comparison of the two voltage curves indicates that the effect of increasing the number of exciting magnets is much more pronounced at higher rotational speeds than at lower speeds. Specifically, the average voltage rises from 17.47 to 31.14 at a speed of 490 rpm and from 2.4 to 3 V at 195 rpm for the one and two-magnet configurations. This behavior is attributed to the increased nonlinearity of the harvester due to the rise in the number of force applications per cycle. The excellent agreement between all three voltage diagrams for both one and two-magnet configurations demonstrates the accuracy of the modeling and the precise design and construction of the experimental setup. The maximum difference between the theoretical and experimental results for the maximum voltage generated by two exciting magnets at a speed of 490 RPM is 13.81%. This discrepancy arises from the reduced strain transfer due to the adhesive at high speeds between the substrate and the piezoelectric layer. Using a more suitable adhesive could help minimize this difference.

6.5. Effect of resistance load on ARPEH

Figure (13) illustrates the maximum voltage and power as a function of load resistance from 1 KΩ to 10 MΩ at three angular velocities and two magnet configurations. In all cases, the voltage increases with the circuit resistance, but the maximum power decreases after reaching its peak at the optimal resistance of 2 MΩ; however, these changes become evident from a resistance of 50 KΩ. Simultaneously, the rotational speed significantly affects the voltage and, consequently, the maximum output power. According to Figure 13(a), as the rotational speed ascends from 1/14 to 1/10 of the harvester's natural frequency, the maximum voltage for n=1 ranges from 19.3-31.2 V, and the maximum power varies between 84.54-225.85 μW. Regarding excitation with two magnets, the respective ranges for voltage and power are 24.75-46.17 V and 147.94-503.73 μW, as shown in Figure 13(b). Therefore, increasing the number of exciting magnets from one to two results in a remarkable 123% increase in power and a 48% increase in maximum voltage. The reasonable alignment between theoretical and experimental results, with a maximum error of 6.6%, demonstrates the research's confidence. This discrepancy is also related to the choice of the approximate mode shape.

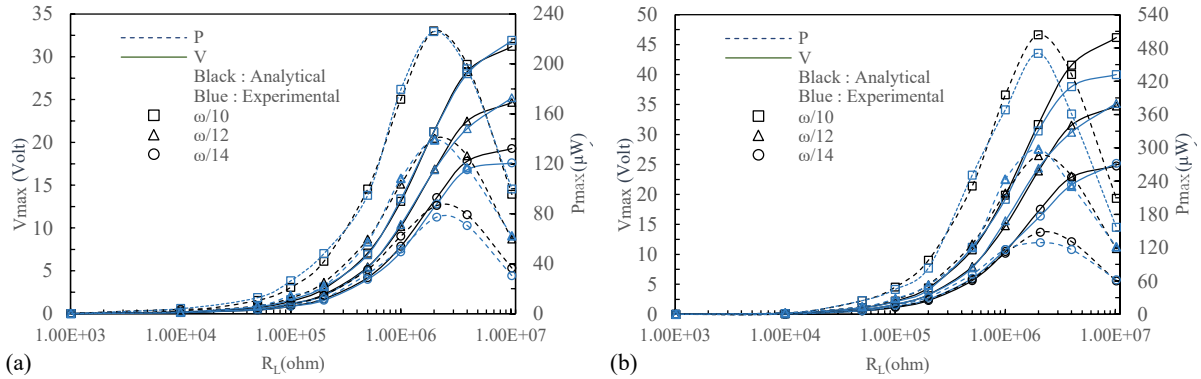

Fig. 13: Max voltage and power output, d_m=10 mm, (a) n_0=1; (b) n_0=2

6.6. Effect of magnetic distance on ARPEH output power

One of the pivotal parameters influencing harvested energy is the distance denoted as dm between the exciting magnet and the excited magnet. When determining this distance, it is imperative to ensure that the maximum displacement of the harvester tip remains reasonably less than the distance between two magnets. Consequently, in configurations with four, two, and one magnets and at rotational speeds of up to 2140 rpm, this distance should be equal to or greater than 10mm.

Table 3 Effect of magnetic distance on ARPEH P_{rms} and P_{Max}, $R_L=R_{L\text{-}Optimum}$, n=ω/16 (Hz)

			d_m (mm)			
			10	**12**	**14**	**16**
n_0=1	**P_{rms}**	Analytical	3.90	1.38	0.55	0.23
		Experimental	3.92	1.28	0.52	0.20
	P_{max}	Analytical	52.17	21.32	9.16	4.11
		Experimental	46.08	19.97	9.02	3.81
n_0=2	**P_{rms}**	Analytical	11.77	4.02	1.49	0.60
		Experimental	9.68	3.92	1.28	0.54
	P_{max}	Analytical	79.63	30.89	12.65	5.43
		Experimental	67.28	36.98	12.30	7.07
n_0=4	**P_{rms}**	Analytical	42.45	12.81	4.49	1.71
		Experimental	35.28	10.58	4.50	1.69
	P_{max}	Analytical	165.80	56.29	21.58	8.82
		Experimental	169.28	54.08	30.42	12.30

Table (3) indicates the impact of this distance on the average and maximum power for three different magnet configurations at $\omega/16$ Hz (245 rpm) rotation speed and optimal resistance of 2 MΩ. As evident, the output power decreases due to the reduction in magnetic force resulting from increased distance. The intensity of this reduction is higher in the configuration with four magnets. However, equal to or beyond a distance of 16 mm, the number of magnets minimally impacts the output power. Experimental results also confirm the effect of this distance.

6.7. Frequency sweep response

The main objective of this project is to improve energy harvesting at lower frequencies. For this purpose, the experimental investigation has focused on assessing the impact of the number and spacing of magnets on the output voltage within a specific range of angular velocities. The experiments involve a linear increase in angular velocity from 0 to a maximum of 25 Hz, slightly exceeding 1/3 of the natural frequency of the harvester. Furthermore, the distance between magnets varies in three scenarios: 10, 12, and 14 millimeters. The results of these experiments are detailed in Figures 14(a), 14(b), and 14(c) for configurations with one, two, and four magnets, respectively. As evident, when the excitation frequency is lower than the natural frequency of the harvester, subharmonic (peaks) emerge in nonlinear systems, leading to the frequency up-conversation phenomenon. Initial results reveal that a decreased distance between magnets increases the output voltage magnitude and the size of voltage signal peaks. According to Figure 14(a), the first peak for the n=1 magnet structure occurs at an angular velocity of 22.10 Hz, approximately 1/3 of the natural frequency of the harvester ($\omega/3 = 21.92$). Subsequent peaks are observed at angular

velocities of 16.28 Hz, 13.0 Hz, 10.9 Hz, and so forth, which are very close to 1/4, 1/5, 1/6, and so on, of the natural frequency of the harvester.
Similarly, for n=2, as illustrated in Figure 14(b), the first, second, and third peaks are observed at 16.57 Hz, 10.84 Hz, and 8.20 Hz, corresponding to 1/4, 1/6, and 1/8 of the natural frequency of the harvester. Likewise, in the case of excitation with four magnets, the first, second, and third peaks occur at angular velocities of 16.61 Hz, 8.29 Hz, and 5.54 Hz, equivalent to 1/4, 1/8, and 1/12 of the natural frequency of the harvester. Consequently, in a harvester consisting of j-rotating magnets, the rotational speed at which subharmonic peaks in the voltage signal will occur is given in Equation 29.

$$n_j = \frac{\omega}{jn_0} \tag{29}$$

In this expression, n_j denotes the angular velocity of the j^{th} subharmonic. Figure 14(d) illustrates these results with a magnet distance dm=10 mm and n0=1,2,4 for a more comprehensive comparison. It is observed that increasing the number of exciting magnets changes the maximum voltage significantly so that at an angular velocity of ω/4=16.44 Hz (ω=986 rpm), the voltage peak in excitation with two and four magnets increases by 16% and 100%, respectively, compared to excitation with one magnet. This enhancement is justified because the oscillation amplitude and output voltage increase as the rotational speed approaches the harvester's natural frequency. In the case of excitation with four magnets and at an angular velocity of 16.44 Hz, the value of $nj \cdot j \cdot n_0$ equals 65.78 Hz. This value corresponds to the natural frequency of the harvester, at which the maximum output voltage is extracted. Therefore, the increase in the number of magnets enables the design of a harvester capable of extracting more energy at low rotational speeds.

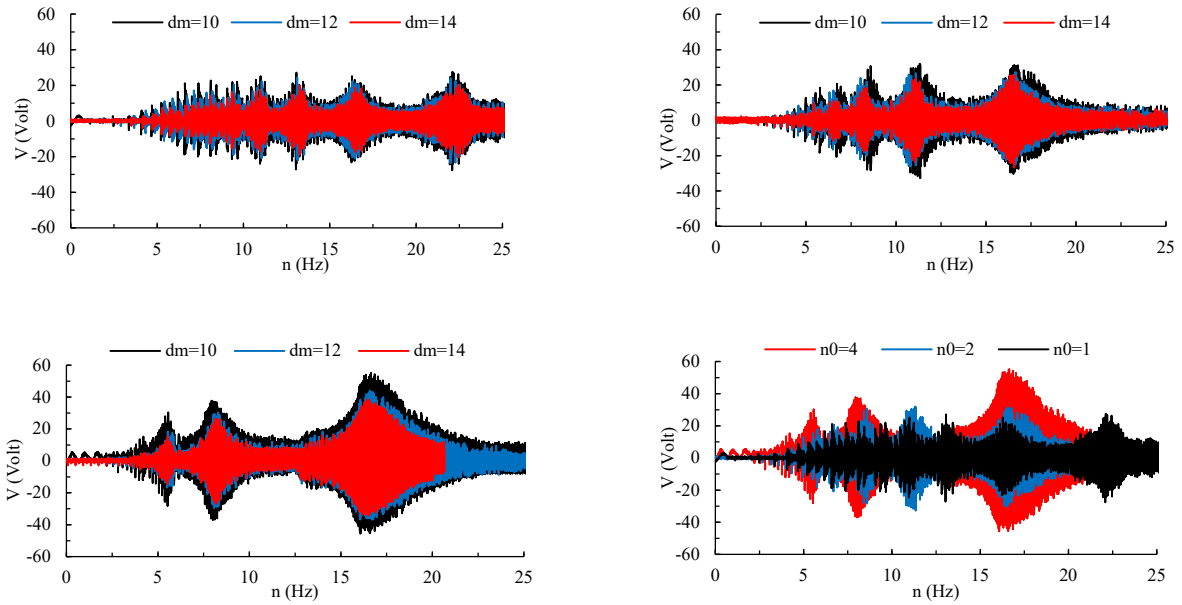

Fig. 14: Measured voltage output versus angular velocity, RL=RL-Optimum
(a) n0=1; (b) n0=2; (c) n0=4 (d); dm=10 mm

6.8. Summary comparison for rotational piezoelectric energy harvesting

After examining various parameters, it has become evident that reducing the distance between magnets and increasing the number of exciting magnets contributes to augmenting the harvester's output power. However, it is crucial to recognize that the distance should be, at most, the maximum displacement of the beam's end. Furthermore, increasing the number of magnets proves effective up to a certain threshold, beyond which it induces a reduction in the displacement of the beam's end, subsequently decreasing strain and output voltage. According to the theoretical model, considering the harvester's geometry in this study, the maximum possible number of exciting magnets to achieve maximum efficiency and harvesting at low frequencies can be four. Consequently, with four magnets and $d_m = 10\ mm$, the ultimate test for extracting maximum power at the optimal resistance was carried out. In this configuration, at an angular velocity of ω/2=16.43 Hz (ω=986 rpm), the energy harvester yielded a maximum power output of 1523.5 μW.

Table 4 Summary comparison for piezoelectric energy harvesting.

	Ref.	Piezo dimension (mm)	Piezo shape	Material type used	rpm	Voltage at max power (Volt)	Max power (μW)	Power density (μW/mm^3)	Mechanical power source
1	[30]	Φ20 -15×0.5	Arc	PZT	-	32	4080	8.65	Base excitation
2	[32]	Φ20 -8×0.11	Arc	PVDF	-	17	49	1.88	Base excitation
3	[50]	150×20×0.2	Rectangle	PVDF	504	14.16	1003	1.67	Rotation
4	[51]	22×6×0.5	Rectangle	PVDF	700	21.5	140	2.12	Rotation
5	[52]	25×12×0.1	Rectangle	PVDF	965	4.6	36	1.20	Rotation-magnet
6	[11]	33.5×2×0.15	Rectangle	PZT	660	2.8	52.3	5.2	Rotation-magnet
7	[23]	Φ20 -8 (8 Number)	Circle	PZT	1500	19	3500	9.67	Rotation-magnet
8	Present	Φ21.3 - 20×0.11	Arc	PVDF	1264	26.8	359.1	2.68	Rotation-1 magnet
					986	31.7	487	3.75	Rotation-2 magnet
					489	36.81	677.5	5.10	Rotation-4 magnet
					986	55.2	1523.5	11.37	Rotation-4 magnet

Table (4) presents a comprehensive comparison of various parameters influencing the performance of the piezoelectric energy harvester, encompassing dimensions, geometry, piezoelectric material, rotational speed, and voltage. Depending on these parameters, the maximum power and output power density are delineated for different sources and the present study. Notably, the power density of the current system at lower rotational speeds, particularly during excitation with four magnets, significantly surpasses the values reported in the literature referenced. Consequently, the system designed in this study demonstrates a superior capability for application in consumer-oriented scenarios.

7. Conclusion

This article introduces a novel approach to enhance the performance of rotational energy harvesters by replacing flat piezoelectric elements with curved ones. The proposed design, incorporating magnetic force, also enhances the frequency flexibility of the harvester. The energy harvesting system comprises a rotating disc accommodating up to eight exciting magnets, a curved beam, a layer of polymer piezoelectric material, a beam tip magnet, and a resistance load. The electromechanical behavior of the harvester is described by derived equations using the energy method, incorporating a nonlinear restoring force with softening behavior. The approximate mode shape is employed to extract the mass coefficients, damping, and electromechanical coupling terms. A new correction factor for displacement and time-dependent magnetic force has been introduced to enhance the theoretical model's accuracy. This factor depends on the number of exciting magnets, and its increase, due to the enhanced displacement of the harvester's end and consequently the reduction of the minimum distance between the magnets, leads to an increase in the correction factor. Finally, the experimental model constructed fully conformed with the theoretical model, and various results have been extracted and compared. The high level of compliance with these two approaches' results indicates the high accuracy of this designed system. Increasing the rotational speed of the exciting magnets enhances the maximum, average, and peak-to-peak voltage. However, the percentage increase is more noticeable in RMS and usable voltage. The addition of exciting magnets significantly increases the harvester's output voltage and power while reducing the rotational speed at which maximum power is extracted. The magnetic distance variation strongly influences the harvester's output, with a significant effect at higher numbers of exciting magnets. In the case of four exciting magnets, the system achieves a maximum power of 1523.5 μW and a power density of 11.37 μW/mm³, demonstrating a substantial improvement over other research. Due to the frequency up-conversion phenomenon and the presence of superharmonics, this harvester is recommended for use in all rotational energy harvesting systems with varying rotational speeds, such as wind and water. Consequently, Further enhancement of this harvester's energy extraction capabilities is possible with the simultaneous installation of eight beams with two piezoelectric layers.

Declaration of competing interest

The authors declare that they have no known competing financial interests or personal relationships that could have appeared to influence the work reported in this paper.

Acknowledgments

The authors would like to express their gratitude to the mechanical engineering workshop and laboratory of Golpayegan Faculty of Engineering, which was supervised by Engineer D. Jalili and Engineer HR. Masoumi, for their assistance in preparing the laboratory equipment.

Appendix A

The magnetic force for the magnetic interaction was derived in Maple using Equations (16-19). The parameters $A_1 - A_5$ are expressed as,

$$\begin{aligned} A_1 &= a/2 - d_A \cos\beta \\ A_2 &= R_A + w(L,t) - d_A \sin\beta \\ A_3 &= R_B \cos\alpha \\ A_4 &= R_B \sin\alpha \\ A_5 &= A_1^2 + A_3^2 + (A_2 - A_4)^2 \end{aligned} \tag{A1}$$

where

$$\begin{aligned} R_B &= R_D + h_B \\ R_A &= R_D + h_A + h_B + d_m \\ d_A &= \sqrt{\left(\frac{a}{2}\right)^2 + h_A^2} \\ \kappa &= arctan\left(\frac{2h_A}{a}\right) \\ \beta &= \kappa + \left(\frac{w(L,t)}{2R+a} - \upsilon\right) \\ \gamma &= \beta - \kappa \end{aligned} \tag{A2}$$

The geometric parameters in Equation (26) are [41]:

$$h_{pc} = \frac{(E_s/E_p)h_s\left(h_p + h_s\right)}{2(h_p + (E_s/E_p)h_s)} \tag{A3}$$

References

[1] R. Ramezanpour, H. Nahvi, S. Ziaei-Rad, A vibration-based energy harvester suitable for low-frequency, high-amplitude environments: Theoretical and experimental investigations, Journal of Intelligent Material Systems and Structures, 27 (2015) 642-665.

[2] J.Y. Cho, J.Y. Choi, S.W. Jeong, J.H. Ahn, W.S. Hwang, H.H. Yoo, T.H. Sung, Design of hydro electromagnetic and piezoelectric energy harvesters for a smart water meter system, Sensors and Actuators A: Physical, 261 (2017) 261-267.

[3] S.P. Machado, M. Febbo, J.M. Ramírez, C.D. Gatti, Rotational double-beam piezoelectric energy harvester impacting against a stop, Journal of Sound and Vibration, 469 (2020) 115141.

[4] K.-J.I. Egbe, A. Matin Nazar, P. Jiao, Piezoelectric-triboelectric-electromagnetic Hybrid Rotational Energy Harvesters (H-REH), International Journal of Mechanical Sciences, 235 (2022) 107722.

[5] Y.C. Lo, Y.C. Shu, Self-powered SECE piezoelectric energy harvesting induced by shock excitations for sensor supply, Mechanical Systems and Signal Processing, 177 (2022) 109123.

[6] S. Fang, K. Chen, Z. Lai, S. Zhou, W.-H. Liao, Analysis and experiment of auxetic centrifugal softening impact energy harvesting from ultra-low-frequency rotational excitations, Applied Energy, 331 (2023) 120355.

[7] S.X. Long, S.Y. Khoo, Z.C. Ong, M.F. Soong, Y.-H. Huang, N. Prasath, S. Noroozi, A comprehensive review on mechanical amplifier structures in piezoelectric energy harvesters, Mechanics of Advanced Materials and Structures, (2023) 1-30.

[8] A. Bartasyte, G. Clementi, Q. Micard, I. Labbaveettil, A.S.L. Moreira, S. Boujnah, M. Ouhabaz, A. Verma, A. Ichangi, G. Malandrino, S. Mathur, B. Dulmet, S. Margueron, Material strategies to enhance the performance of piezoelectric energy harvesters based on lead-free materials, Journal of Micromechanics and Microengineering, 33 (2023) 053001.

[9] X. Zheng, L. He, S. Wang, X. Liu, R. Liu, G. Cheng, A review of piezoelectric energy harvesters for harvesting wind energy, Sensors and Actuators A: Physical, 352 (2023) 114190.

[10] P. Firoozy, S.E. Khadem, S.M. Pourkiaee, Power enhancement of broadband piezoelectric energy harvesting using a proof mass and nonlinearities in curvature and inertia, International Journal of Mechanical Sciences, 133 (2017) 227-239.

[11] H. Fu, E.M. Yeatman, Rotational energy harvesting using bi-stability and frequency up-conversion for low-power sensing applications: Theoretical modelling and experimental validation, Mechanical Systems and Signal Processing, 125 (2019) 229-244.

[12] U. Bartsch, J. Gaspar, O. Paul, Low-frequency two-dimensional resonators for vibrational micro energy harvesting, Journal of Micromechanics and Microengineering, 20 (2010) 035016.

[13] C. Minh Tri Tien, N. Seo Goo, Use of a piezo-composite generating element for harvesting wind energy in an urban region, Aircraft Engineering and Aerospace Technology, 82 (2010) 376-381.

[14] B. Maamer, A. Boughamoura, A.M.R. Fath El-Bab, L.A. Francis, F. Tounsi, A review on design improvements and techniques for mechanical energy harvesting using piezoelectric and electromagnetic schemes, Energy Conversion and Management, 199 (2019) 111973.

[15] Y. Cao, J. Yang, D. Yang, Coupling nonlinearities investigation and dynamic modeling of a tristable combined beam rotational energy harvesting system, Mechanical Systems and Signal Processing, 200 (2023) 110503.

[16] X. Wang, Q. Du, Y. Zhang, F. Li, T. Wang, G. Fu, C. Lu, Dynamic characteristics of axial load bi-stable energy harvester with piezoelectric polyvinylidene fluoride film, Mechanical Systems and Signal Processing, 188 (2023) 110065.

[17] H. Mohammad Khanlo, R. Dehghani, The effect of distance and dimensions of magnets on nonlinear behavior of piezomagnetoelastic bimorph energy harvester, Journal of Theoretical and Applied Vibration and Acoustics, 4 (2018) 37-64.

[18] J.H. Yang, M.A.F. Sanjuán, H.G. Liu, Vibrational subharmonic and superharmonic resonances, Communications in Nonlinear Science and Numerical Simulation, 30 (2016) 362-372.

[19] I. Sari, T. Balkan, H. Külah, An Electromagnetic Micro Power Generator for Low-Frequency Environmental Vibrations Based on the Frequency Upconversion Technique, Journal of Microelectromechanical Systems, 19 (2010) 14-27.

[20] H. Fu, E.M. Yeatman, A methodology for low-speed broadband rotational energy harvesting using piezoelectric transduction and frequency up-conversion, Energy, 125 (2017) 152-161.

[21] W.-H. Wu, K.-C. Kuo, Y.-H. Lin, Y.-C. Tsai, Non-contact magnetic cantilever-type piezoelectric energy harvester for rotational mechanism, Microelectronic Engineering, 191 (2018) 16-19.

[22] A.G. Paulo e Silva, J.M. Basílio Sobrinho, C. da Rocha Souto, A. Ries, A.C. de Castro, Design, modelling and experimental analysis of a piezoelectric wind energy generator for low-power applications, Sensors and Actuators A: Physical, 317 (2021) 112462.

[23] M. Rizal, Husni, A.Z. Mubarak, M. Dirhamsyah, Arhami, Design and experimental study of a piezoelectric energy harvester embedded in a rotating spindle excited by magnetic force, Sensors and Actuators A: Physical, 340 (2022) 113521.

[24] Y. Cao, J. Yang, D. Yang, A magnetic excitation enhanced energy harvester with combined beam for rotational motion, Sensors and Actuators A: Physical, 360 (2023) 114569.

[25] J. Baker, S. Roundy, P. Wright, Alternative Geometries for Increasing Power Density in Vibration Energy Scavenging for Wireless Sensor Networks, in: 3rd International Energy Conversion Engineering Conference, 2012.

[26] S. Ben Ayed, A. Abdelkefi, F. Najar, M.R. Hajj, Design and performance of variable-shaped piezoelectric energy harvesters, Journal of Intelligent Material Systems and Structures, 25 (2013) 174-186.

[27] H. Salmani, G.H. Rahimi, S. Saraygord Afshari, Optimization of the shaping function of a tapered piezoelectric energy harvester using tabu continuous ant colony system, Journal of Intelligent Material Systems and Structures, 30 (2019) 3025-3035.

[28] K. Mohamed, H. Elgamal, S.A. Kouritem, An experimental validation of a new shape optimization technique for piezoelectric harvesting cantilever beams, Alexandria Engineering Journal, 60 (2021) 1751-1766.

[29] C. Martinelli, A. Coraddu, A. Cammarano, Performance-aware design for piezoelectric energy harvesting optimisation via finite element analysis, International Journal of Mechanics and Materials in Design, 19 (2023) 121-136.

[30] Z. Yang, Y.Q. Wang, L. Zuo, J. Zu, Introducing arc-shaped piezoelectric elements into energy harvesters, Energy Conversion and Management, 148 (2017) 260-266.

[31] T.Q. Thai, X. Zhuang, T. Rabczuk, Curved flexoelectric and piezoelectric micro-beams for nonlinear vibration analysis of energy harvesting, International Journal of Solids and Structures, 264 (2023) 112096.

[32] X. Chen, X. Zhang, L. Wang, L. Chen, An arch-linear composed beam piezoelectric energy harvester with magnetic coupling: Design, modeling and dynamic analysis, Journal of Sound and Vibration, 513 (2021) 116394.

[33] A.V. Krishnanunni, N. Kaur, S. Bhalla, N. Singh, S. Balguvhar, Efficacy of singly curved thin piezo transducers for structural health monitoring and energy harvesting for RC structures, Energy Reports, 9 (2023) 2506-2524.

[34] A.A. Jafari, I. Fakhari Golpayegani, Design and analysis of an exponentially tapered piezoelectric energy harvester under nonlinear rotational indirect magnetic excitation, Proceedings

of the Institution of Mechanical Engineers, Part C: Journal of Mechanical Engineering Science, 238 (2024) 1-16.

[35] W.-S. Jung, M.-J. Lee, M.-G. Kang, H.G. Moon, S.-J. Yoon, S.-H. Baek, C.-Y. Kang, Powerful curved piezoelectric generator for wearable applications, Nano Energy, 13 (2015) 174-181.

[36] W. Zhou, B. Wang, C.W. Lim, Z. Yang, A distributed-parameter electromechanical coupling model for a segmented arc-shaped piezoelectric energy harvester, Mechanical Systems and Signal Processing, 146 (2021) 107005.

[37] J. Ding, M. Lu, A. Deng, S. Jiang, A piezoelectric energy harvester using an arc-shaped piezoelectric cantilever beam array, Microsystem Technologies, 28 (2022) 1947-1958.

[38] X. Chen, X. Zhang, Y. Guo, F. Zhu, Modeling and performance analysis of a curve-shaped based doubly clamped piezoelectric energy harvester (CD-PEH), Journal of Intelligent Material Systems and Structures, (2023) 1045389X231181493.

[39] M. Shang, W. Qin, H. Li, Q. Liu, H. Wang, Harvesting vibration energy by novel piezoelectric structure with arc-shaped branches, Mechanical Systems and Signal Processing, 200 (2023) 110577.

[40] M. Hasani, M. Khazaee, J.E. Huber, L. Rosendahl, A. Rezania, Design and analytical evaluation of an impact-based four-point bending configuration for piezoelectric energy harvesting, Applied Energy, 347 (2023) 121461.

[41] A. Erturk, D.J. Inman, A Distributed Parameter Electromechanical Model for Cantilevered Piezoelectric Energy Harvesters, Journal of Vibration and Acoustics, 130 (2008) 041002.

[42] J. Kan, C. Fan, S. Wang, Z. Zhang, J. Wen, L. Huang, Study on a piezo-windmill for energy harvesting, Renewable Energy, 97 (2016) 210-217.

[43] M.A. Karami, J.R. Farmer, D.J. Inman, Parametrically excited nonlinear piezoelectric compact wind turbine, Renewable Energy, 50 (2013) 977-987.

[44] K.W. Yung, P.B. Landecker, D.D. Villani, An Analytic Solution for the Force Between Two Magnetic Dipoles, Magnetic and Electrical Separation, 9 (1998) 39-52.

[45] H.-X. Zou, W.-m. Zhang, W.-B. Li, K.-X. Wei, Q.-H. Gao, Z.-K. Peng, G. Meng, Design and experimental investigation of a magnetically coupled vibration energy harvester using two inverted piezoelectric cantilever beams for rotational motion, Energy Conversion and Management, 148 (2017) 1391-1398.

[46] J. Kan, Y. Wu, S. Li, S. Wang, Z. Zhang, A tunable rotational energy harvester exploiting a flexible-clamping piezoelectric beam by deploying magnetic repulsive force, Sensors and Actuators A: Physical, 353 (2023) 114198.

[47] X. Zhang, Y. Wenjuan, Z. Meng, T. Houzhi, F. Hongwei, M. Qinghua, W. Xiang, An Arc-Shaped Piezoelectric Bistable Vibration Energy Harvester: Modeling and Experiments, Sensors, 18 (2018) 4472.

[48] S. Zhou, J. Cao, D.J. Inman, J. Lin, S. Liu, Z. Wang, Broadband tristable energy harvester: Modeling and experiment verification, Applied Energy, 133 (2014) 33-39.

[49] Uniaxially stretched piezo PVDF film, in: P. Technologies (Ed.) PKS--P0110-Pin-001, PolyK Technologies, Pennsylvania, USA, 2023, pp. 1.

[50] X. Rui, Y. Li, X. Zheng, Z. Sha, Z. Zeng, Design and experimental study of a piezoelectric energy harvester in automotive spokes, Journal of Physics D: Applied Physics, 52 (2019) 355501.

[51] W. Yu-Jen, C. Tsung-Yi, Y. Jui-Hsin, Design and kinetic analysis of piezoelectric energy harvesters with self-adjusting resonant frequency, Smart Materials and Structures, 26 (2017) 095037.

[52] X. Wu, M. Parmar, D.W. Lee, A Seesaw-Structured Energy Harvester With Superwide Bandwidth for TPMS Application, IEEE/ASME Transactions on Mechatronics, 19 (2014) 1514-1522.